



# Low-cost, scale production of nanocellulose from bamboo wastes via a recyclable and stable strategy

Hanfei Zhao<sup>1,2</sup> · Longfei Sun<sup>1,2</sup> · Yucong Yu<sup>1</sup> · Jing Lu<sup>1</sup> · Xinxin Chen<sup>1</sup> · Lin Liu<sup>1,2</sup>

Received: 20 January 2024 / Revised: 2 April 2024 / Accepted: 15 April 2024

© The Author(s), under exclusive licence to Springer-Verlag GmbH Germany, part of Springer Nature 2024

## Abstract

Green and sustainable nanocellulose shows the great application potential in various fields due to its unique advantages and performances; thereby, the low cost, stable, and scale production of nanocellulose is urgent but still a challenge. Here, a recyclable and stable strategy was developed to simultaneously produce carboxylic cellulose nanocrystals (CNC) and cellulose nanofibers (CNF) from waste bamboo pulp (WBP) through oxalic acid dihydrate (OAD) hydrolysis and subsequent homogenization. In this strategy, OAD was recrystallized and reused for WBP hydrolysis to evaluate the recyclability, reliability, and economic viability. Response surface methodology (RSM) was performed to optimize experimental variables, and achieving the optimum conditions with hydrolysis time of 5.1 h, temperature of 92 °C, and OAD content of 1.65 g/mL. Importantly, after four recrystallization-reuse cycles, OAD still retained admirably hydrolytic reactivity and efficiency, no significant variation on the yield, structure, and thermal stability of the obtained CNC. Benefiting from the applicability and reliability of the proposed strategy, the total yield of CNC and CNF in the pilot production was more than 90%. The produced CNC and CNF had high crystallinity with CrI of 85.6 and 80.3%, and high carboxyl group contents of 0.38 and 0.26 mmol/g, respectively. Moreover, OAD recycle significantly reduced the production costs to original 38.9%. Therefore, this work not only provides a low cost, recyclable, and stable approach for manufacturing CNC and CNF but also provides high-performance nanocellulose contributing to the high-value-added applications.

**Keywords** Nanocellulose · Pilot-scale production · Response surface methodology · Surface carboxylation · Recycling stability and reliability · Low cost

## 1 Introduction

In recent years, green and sustainable nanocellulose displayed the great potential applications in nanocomposites [1], flexible electronics [2], battery diaphragm [3], energy storage [4], electromagnetic shielding [5], intelligent packaging [6], biomedical [7], and tissue engineering [8] owing to its unique advantages of high strength, high crystalline, low thermal conductivity, large surface area, surface chemical tunability, biocompatibility, and biodegradability [9, 10]. Therefore, the development of green preparation approach

of nanocellulose has been an interest in both science and industry fields [11].

The current methods for commercial preparation of nanocellulose are mainly focused on acid or enzymatic hydrolysis, oxidation method, mechanical treatment, and combined methods [12, 13]. Among these approaches, 64 wt% sulfuric acid hydrolysis had been considered to be an efficient strategy of producing cellulose nanocrystal (CNC), but with the challenges of complex process, equipment corrosion, high chemical consumption, and low thermal stability of products [14]. Importantly, the large amount of water and acid wastes are difficult to be recycled. To solve these problems, organic acids are exploited to produce nanocellulose in view of its full recyclability. For example, Chen et al. used oxalic acid, maleic acid, and concentrated p-toluenesulfonic acid to extract CNC from bleached kraft eucalyptus pulp and compared their efficiency, founding that oxalic acid possessed the highest yield of 24.7% at 100 °C for 60-min hydrolysis [15]. Ji et al. combined concentrated citric acid

✉ Lin Liu  
linliu@zstu.edu.cn

<sup>1</sup> School of Materials Science and Engineering, Zhejiang Sci-Tech University, Hangzhou 310018, China

<sup>2</sup> Zhejiang Provincial Innovation Center of Advanced Textile Technology, Shaoxing 312000, China

(80%) and mechanically processing to prepare CNC and cellulose nanofiber (CNF) from bagasse pulp with CNC yield of 32.2% at 100 °C for 4-h hydrolysis [16]. Recently, Jiang et al. proposed a two-step strategy of extracting lignin-containing CNC (LCNC) from thermomechanical pulp using molten oxalic acid dihydrate at 110 °C for 30-min hydrolysis, followed by microfluidization. The CNC yield reached up to 70%, and the obtained LCNC exhibits a high degree of uniformity and good thermal stability [17]. Although much progress has been made, relatively low yield of CNC was one of the limitations owing to the insufficient hydrolysis because of weak acidity, or high temperature (~ 110 °C) was carried out to prepare CNC with high yield.

In this work, we developed a recyclable and stable strategy to simultaneously produce carboxylic CNC and CNF in the large scale from waste bamboo pulp (WBP) using recyclable oxalic acid dihydrate (OAD). OAD is a dicarboxylic acid and crystalline solid, which can modify cellulose with carboxylic groups through Fischer-Speier esterification during the hydrolysis process [15, 18] and can be recycled from hydrolysate by simple recrystallization. However, the weak acidity of OAD conventionality resulted in low yield of CNC; thus, chromium chloride is employed as a Lewis acid for assisted hydrolysis to achieve high yield. The effect of OAD feedstocks, reaction time, and temperature on the yield of CNC and CNF was investigated and optimized through response surface methodology (RSM). Moreover, in order to estimate the reliability and applicability of the designed preparation procedure, the variation on the yield, morphology, surface characteristic, chemical structure, crystal structure, and thermal stability of CNC was firstly investigated withstanding four recrystallization-reuse cycles of OAD. Further, pilot scale production of CNC and CNF was conducted, and the energy consumption and feedstock cost were statistically analyzed.

## 2 Experimental section

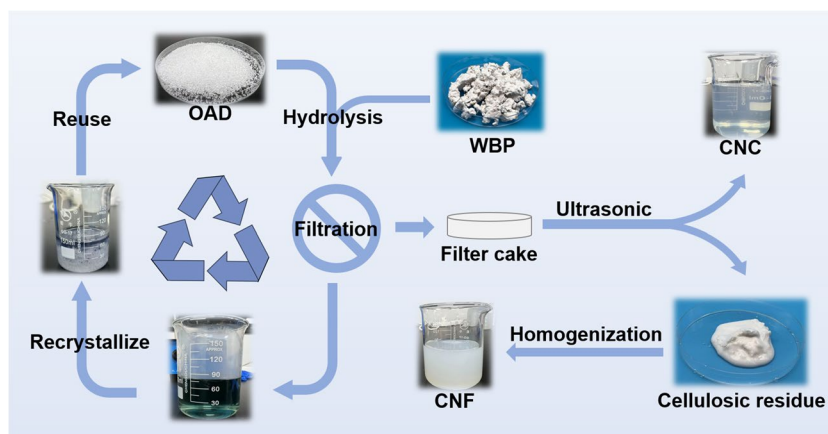
### 2.1 Materials

Waste bamboo pulp (WBP) with cellulose, hemicellulose, and lignin contents of 91.3%, 1.2%, and 4.6%, was provided by QTH Paper Industry Co., Ltd. (Guizhou, China). Chromium chloride hexahydrate ( $\text{CrCl}_3 \cdot 6\text{H}_2\text{O}$ , AR), oxalic acid dihydrate (OAD, 99.5%, AR), NaOH (97%), and HCl (37%) were purchased from Macklin (Shanghai, China).

### 2.2 Production of nanocellulose

Nanocellulose was prepared via a chemi-mechanical synergy strategy. In brief, 1 g of WBP was mixed with 30 mL of OAD/ $\text{CrCl}_3$  solution and hydrolyzed at 80–100 °C for 4–6 h with mechanical stirring of 400 rpm. The feedstock of OAD was 40, 50, and 60 g, and the content of  $\text{CrCl}_3$  was controlled at 0.02 mmol/g to OAD. After hydrolysis, 30 mL of preheated deionized water was added to terminate the reaction. The obtained mixture was filtered, the filtrate was recrystallized for OAD recovery, and the cellulose slurry was dialyzed (MWCO = 8000–14,000) until neutral. Finally, CNC suspension was harvested via ultrasonication (JY99-IIDN, Scientz Biotechnology Co. Ltd., Ningbo, China) under 800 W power for 10 min, and subsequent centrifugation at 6000 rpm for 10 min. Residual solid could be processed into CNF by a high-pressure homogenizer (AH08-100 plus, ATS Engineering Limited Co. Ltd., Suzhou, China). The preparation process is presented in Fig. 1. In order to estimate the practicability of the preparation procedure, recycling process was performed, in which recrystallized OAD was reused for WBP hydrolysis treatment via the same process. According to the number of recycling process, the used OAD and the product were coded as OAD-Rx and CNC-Rx ( $x = 0, 1, 2, 3, 4$ ), respectively.

**Fig. 1** Schematic diagram of CNC and CNF preparation via recyclable OAD hydrolysis



According to the above optimal conditions, the pilot scale production was enlarged to 30 L and conducted in a customized 50-L reactor (HJ-50-LR, Shanghai HJLab Instruments Co., LTD., Shanghai, China). After hydrolysis reaction, cellulose slurry was filtered by the reactor equipped filter plant and washed until neutral. Then the diluent (1 wt%) was ultrasonicated for 1 h at 3000 W power, and stood for 6 h to acquire CNC suspension. CNF was obtained from sediment by homogenization treatment.

### 2.3 Response surface methodology

RSM in a  $3^3$  Box-Behnken design (BBD) factorial design was conducted to optimize experimental variables to maximize CNC yield ( $y$ ) in terms of reaction time ( $X_1$ : 4–6 h), reaction temperature ( $X_2$ : 80–100°C), and OAD content ( $X_3$ : 40–60 g). The experimental variable with their corresponding extreme value is listed in Table 1. Experimental runs of 15 with different sets of variables were acquired using Design Expert 12 software (Static Made Easy, Minneapolis, MN, USA), 12 of which are organized in an analytical factorial design, and 3 of which are replicated at the centroid of the design model to evaluate the pure error variance. Analysis of variance (ANOVA) at 95% confidence interval was employed to assess the significance of individual parameters, the interactions, and the adequacy of predicted model. Coefficient of determination ( $R^2$ ), adjusted  $R^2$ , and predicted  $R^2$  were carried out to assess the quality of second-order polynomial regression model.

### 2.4 Characterization

The yield of nanocellulose was quantified by mass method according to Eq. (1) [19].

$$Y = \frac{C \times V}{m} \times 100\% \quad (1)$$

where  $Y$  is nanocellulose yield (%),  $C$  is nanocellulose content in suspension (g/L),  $V$  is the volume of the obtained nanocellulose suspension (L), and  $m$  is the dry weight of WBP (g).

The surface carboxyl group content of nanocellulose was measured using conductivity titration [20]. Zeta potential of nanocellulose with a diluted concentration of 0.1 wt%

**Table 1** Factors and levels for Box-Behnken independent variables

Code	Factor	Unit	Levels		
			– 1	0	1
$X_1$	Reaction time	h	4	5	6
$X_2$	Reaction temperature	°C	80	90	100
$X_3$	OAD amount	g	40	50	60

was determined using Zetasizer LAB (Malvern Panalytical Ltd., Britain). Dispersion stability of CNC and CNF nanocellulose suspensions (0.5 wt%) was recorded by optical observation after standing for 1 day, 1 week, and 1 month, respectively. The morphology of nanocellulose was observed using TEM (Tecnai 12, FEI Co., the Netherlands) with an accelerating voltage of 100 kV. Fifty samples were randomly selected for size distribution using the statistical software Nano measurer 1.2.0 (Fudan University, Shanghai, China). The chemical structures of WBP and nanocellulose were recorded using ATR-FTIR (Niciletis20, Thermo Fisher Co., Waltham, MA) under 4000–400  $\text{cm}^{-1}$  with a resolution of 4  $\text{cm}^{-1}$  with 32 scans. The thermal stabilities of WBP and nanocellulose were tested by thermogravimetric analyzer (TG209, NETZSCH, Germany) under 50–600 °C with a heating rate of 20 °C/min at  $\text{N}_2$  flow rate of 20 mL/min. The crystal structures of WBP and nanocellulose were characterized by X-ray diffractometer (Empyrean, Malvern Panalytical Ltd., Britain) in the range of  $2\theta = 10$ –60° with a scanning speed of 5°/min. The crystallinity index (CrI) was calculated according to Eq. (2) [21].

$$\text{CrI}(\%) = \frac{I_{200} - I_{\text{am}}}{I_{200}} \times 100\% \quad (2)$$

where  $I_{200}$  and  $I_{\text{am}}$  is the peak intensity of (200) lattice diffraction at  $2\theta = 22.7^\circ$  and amorphous diffraction at  $2\theta = 18.5^\circ$ .

The energy consumption of the pilot production was measured by a multimeter (STSU666, CHINT ELECTRIC Co., Zhejiang, China), and the energy consumption statistics were calculated in the unit of kWh/kg WBP. The residue of  $\text{Cr}^{3+}$  ion in nanocellulose products was detected using inductively coupled plasma spectrometer (ICP, NexION1000, PerkinElmer Instruments Co., Ltd, USA) after digestion [22].

## 3 Results and discussion

### 3.1 Statistical analysis on CNC preparation

CNC and CNF could be extracted via the hydrolysis reaction of WBP using OAD/ $\text{CrCl}_3$  solution. The experimental and predicted CNC yield for the different sets of preparation process to maximize the response variable is tabulated in Table 2. CNC yield varied from 22.61 to 56.58% with an average yield of 40.95%. The highest yield was observed at reaction time of 5 h, reaction temperature of 90 °C, and OAD amount of 50 g.

The experimental data were analyzed by Design Expert 12 software. The relationship between the yield as response variable and the three selected independent

**Table 2** BBD for WBP hydrolysis for maximizing CNC yield

Std	Run	Code levels			CNC yield, $y$ (%)	
		$X_1$	$X_2$	$X_3$	Experimental	Predicted
1	1	-1 (4)	-1 (80)	0 (50)	22.61	21.16
10	2	0 (5)	1 (100)	-1 (40)	51.34	50.52
11	3	0 (5)	-1 (80)	1 (60)	37.98	38.79
6	4	1 (6)	0 (90)	-1 (40)	55.16	54.52
9	5	0 (5)	-1 (80)	-1 (40)	23.78	23.96
5	6	-1 (4)	0 (90)	-1 (40)	41.52	42.79
3	7	-1 (4)	1 (100)	0 (50)	50.68	50.22
4	8	1 (6)	1 (100)	0 (50)	38.76	40.21
7	9	-1 (4)	0 (90)	1 (60)	52.47	53.11
15	10	0 (5)	0 (90)	0 (50)	55.07	55.79
8	11	1 (6)	0 (90)	1 (60)	51.39	50.11
2	12	1 (6)	-1 (80)	0 (50)	39.43	39.89
13	13	0 (5)	0 (90)	0 (50)	56.58	55.79
14	14	0 (5)	0 (90)	0 (50)	55.72	55.79
12	15	0 (5)	1 (100)	1 (60)	41.79	41.61

variables, and their bilinear and quadratic terms are shown in Eq. (3). The positive sign in the equation represents the synergistic effect and the negative sign represents the antagonistic effect.

$$y = 64.12 + 1.65X_1 + 7.6X_2 + 1.26X_3 - 7.44X_1X_2 - 3.99X_1X_3 - 6.19X_2X_3 - 6.77X_1^2 - 19.24X_2^2 - 5.91X_3^2 \quad (3)$$

In the regression equation, statistical significance was determined by the  $F$ -test, and the ANOVA of the influence factors of the fitted model is presented in Table 3. The  $p$ -value of the model is less than 0.0001, suggesting extremely significant.  $P$ -value of the “lack of fit” is 0.1490, more than 0.05, revealing that the “lack of fit” is not significant relative to the pure error. This demonstrates that the selected model is valid in predicting experimental variables and their interaction, and it correlates well with experimental data, it is also proved by the linear relationship presented by the actual and predicted values (Fig. S1). In addition, extremely significant effects ( $p < 0.01$ ) were observed for  $X_1$ ,  $X_2$ ,  $X_1X_2$ ,  $X_1X_3$ ,  $X_2X_3$ ,  $X_1^2$ , and  $X_2^2$ , while  $X_3$  and  $X_3^2$  were significant ( $p < 0.05$ ), and the model did not contain non-significant term. And these variables were not equally important on CNC yield with an order of priority: reaction temperature > reaction time > OAD content. Moreover, high  $R^2 = 0.9934$  and adjusted  $R^2 = 0.9816$  both indicate the experimental variables for CNC extraction can be described by the proposed second-order polynomial equation model. The adequate precision was high to 28.2757, and the difference between predicted and adjusted  $R^2$  values is less than 0.2, which indicates that the predicted values are highly consistent with the actual

**Table 3** ANOVA for CNC yield model regression

Source	Sum of squares	df	Mean square	$F$ -value	$p$ -value
Model	1704.71	9	189.41	84.17	< 0.0001
$X_1$	38.11	1	38.11	16.93	0.0092
$X_2$	431.74	1	431.74	191.85	< 0.0001
$X_3$	17.49	1	17.49	7.77	0.0385
$X_1X_2$	206.50	1	206.50	91.76	0.0002
$X_1X_3$	54.17	1	54.17	24.07	0.0045
$X_2X_3$	141.02	1	141.02	62.66	0.0005
$X_1^2$	39.09	1	39.09	17.37	0.0088
$X_2^2$	794.21	1	794.21	352.92	< 0.0001
$X_3^2$	21.29	1	21.29	9.46	0.0276
Residual	11.25	5	2.25		
Lack of fit	10.10	3	3.37	5.87	0.1490
Pure error	1.15	2	0.5737		
Cor total	1715.96	14			
Std. dev.				$R^2$	0.9934
Mean	44.95			Adjusted $R^2$	0.9816
C.V. %	3.34			Predicted $R^2$	0.9043
				Adeq Precision	28.2757

values. In summary, the proposed regression model can be used to accurately analyze and predict CNC yield as a guide for actual production.

### 3.2 RSM and optimum conditions

In general, response surface plots provide a more intuitive response to the combined effects of the variables on



the response term and identify the type of interaction [23]. Based on the regression equations, 3D model plots and 2D contour plots of the effects of the interaction between the factors on CNC yield were obtained, as shown in Fig. 2. Each plot shows the extent to which the other two variables affect the response term when one variable is at level zero. In Fig. 2a, d, the trend in yield is steeper when the reaction time is constant and the reaction temperature is varied as opposed to changing the reaction time by holding the reaction temperature constant. This indicated that reaction temperature had a more significant effect than time which is consistent with the results in Table 3. At low reaction temperature (80 °C), CNC yield increased with the reaction time, but was less than 50%, revealing the lower temperature level was not enough to motivate the penetration of protons and catalysts in reaction system into cellulose fibers [23]. Increasing reaction temperature to 90–95 °C and reaction time was extended to around 5 h, the yield reached a great value. The interaction effect of reaction time and OAD content on yield is shown in Fig. 2b, e, and displayed the highest yield when the reaction time was 5.0–5.5 h and OAD content was around 50 g; thereafter, the yield decreased with the increase of either time or OAD content. Excessive OAD content and reaction time were prone to the breakage of  $\beta$ -1,4-glycosidic bonds in cellulose chains, even hydrolyzing cellulose into glucose, leading to low CNC yields [24]. Similarly, Fig. 2c, f suggests the significant interaction between reaction temperature and OAD content. As the increase of reaction temperature, the

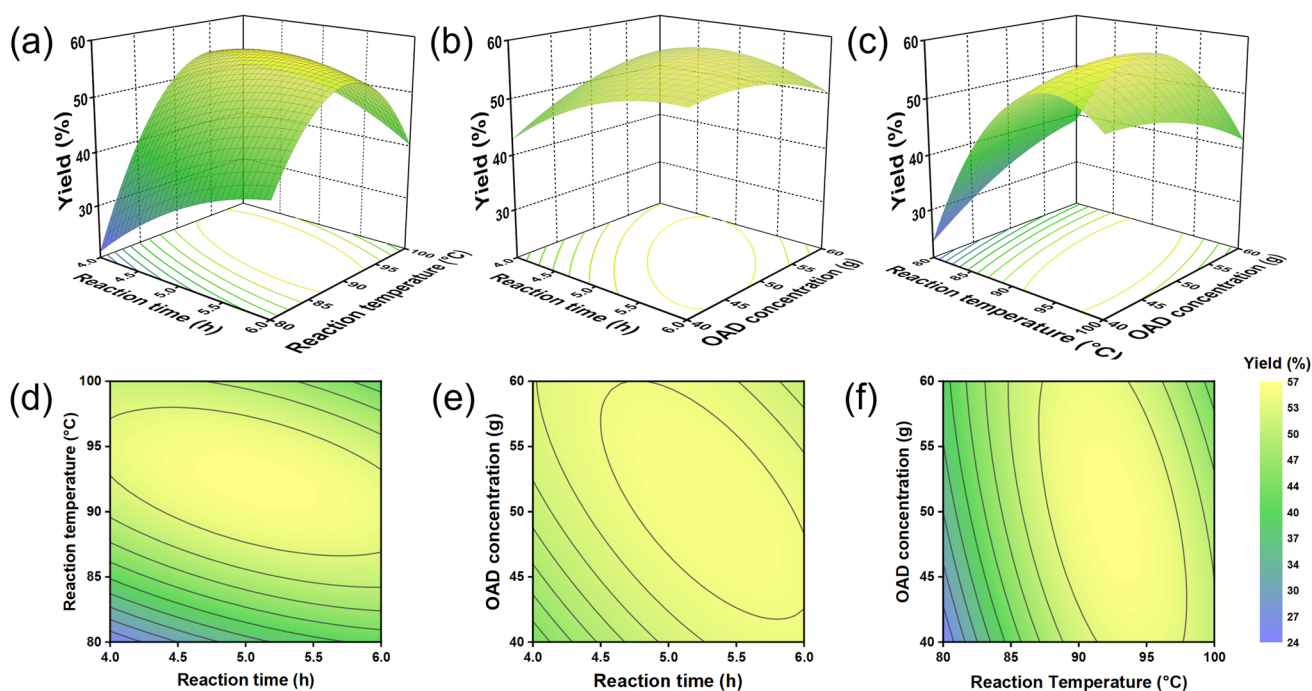
proton dissociation of OAD was promoted as well as Lewis acid ( $\text{CrCl}_3$ ) diffusion was accelerated, achieving the high CNC yield. However, excessive temperature could cause over-hydrolysis of cellulose, declining the yield.

Combining the equation predictions with the actual experimental conditions, CNC yield reached the maximum value of 58.6% at reaction time of 5.1 h, temperature of 92 °C, and OAD amount of 49.6 g (i.e., 1.65 g/mL content), which was not significantly different from the predicted value (56.7%). The experimental results were close to the response surface predictions, indicating that the predictive model is directive for estimating CNC yields.

### 3.3 Reliability of preparation procedure

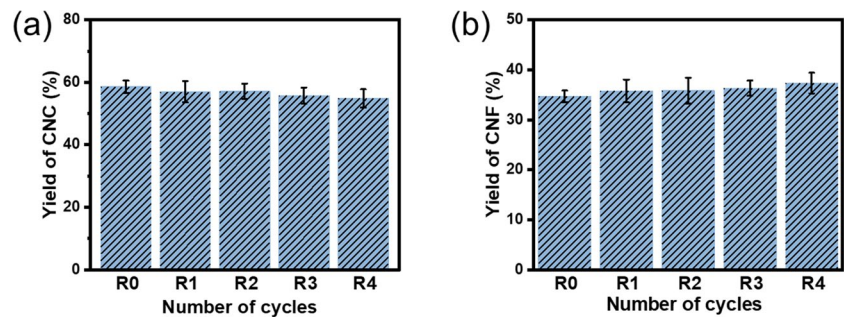
Further, the reliability of the preparation procedure of nanocellulose was evaluated through four recycling processes in which recrystallized OAD (Fig. S2) was reused for WBP hydrolysis treatment under the above optimized conditions, i.e., reaction time of 5.1 h, temperature of 92 °C, and OAD content of 1.65 g/mL. The variation on the yield, morphology, surface characteristic, chemical structure, crystal structure, and thermal stability of nanocellulose was investigated in detail.

Figure 3 shows the effect of cycle numbers of OAD on the yield of CNC and CNF. Clearly, the yield of both CNC and CNF was stable and there was no significant change with up to four cycles of validation. CNC yield could be maintained



**Fig. 2** Response surface analysis on CNC yield with the interaction effect between reaction time and temperature (a, d), reaction time and OAD content (b, e), and reaction temperature and OAD content (c, f)

**Fig. 3** Yield of CNC (a) and CNF (b) with different OAD cycles



at 58.6–54.9%, while 34.7–37.3% of CNF, the total yield of CNC and CNF was more than 92% each cycle. Further, statistical significance tests between groups were performed using ANOVA to assess the cycling stability; the results are presented in Table S1. It could be found that intergroup *p*-values were 0.536 (CNC) and 0.609 (CNF), respectively, suggesting the intergroup difference in yield was not significant. In addition, the variance of the yield both remained at a small value, and did not increase with the cycle numbers of OAD for cellulose hydrolysis. These results confirmed the stability and reliability of the proposed cycling process, which was conducive to the reduction of production costs.

The effect of cycle numbers of OAD on the microstructure of CNC and CNF was investigated. From Fig. 4a, short rod-like CNCs with the average length of  $250 \pm 66$  nm and diameter of  $6.8 \pm 1.8$  nm were achieved. The recycling of

OAD almost did not change the rod-like microstructure of CNC; the size of CNC-R4 slightly declined but still maintained at  $216 \pm 70$  nm of average length and  $6.6 \pm 1.1$  nm of average diameter after four recycles (Fig. 4b). Similar to the case of CNC, no significant difference in the morphology of CNF was observed after four cycles of production, as shown in Fig. 4c, d. Initial CNF-R0 were needle-like nanofibers with the average length of  $569 \pm 113$  nm and diameter of  $9.3 \pm 2.3$  nm, while almost unchanged morphology and size after four recycles.

The dispersion stability of CNC and CNF was also recorded by periodic optical observation. As shown in Fig. 5, the obtained CNC formed a transparent, homogeneous aqueous suspension with a light blue color, while milky suspension was formed by the obtained CNF. CNC and CNF suspensions both were stable and no sedimentation occurred

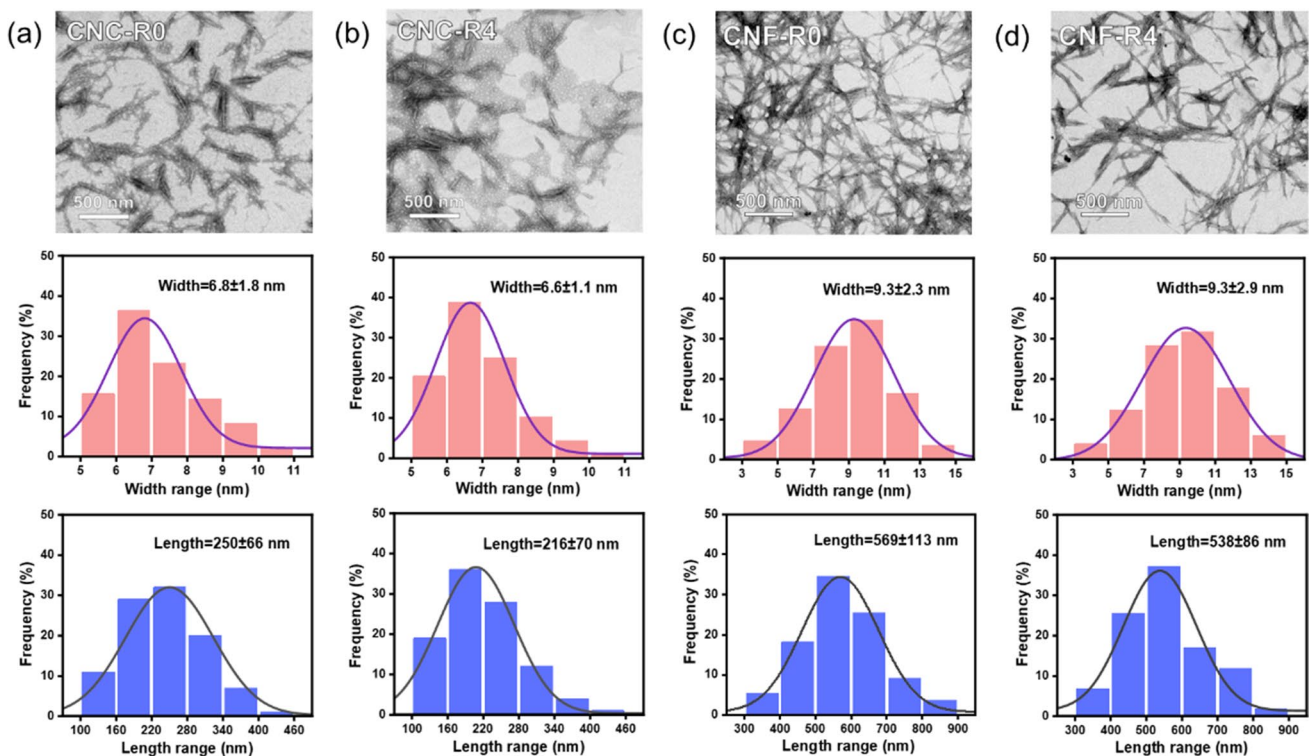


**Fig. 4** TEM images and size distribution of CNC and CNF before and after 4th cycles

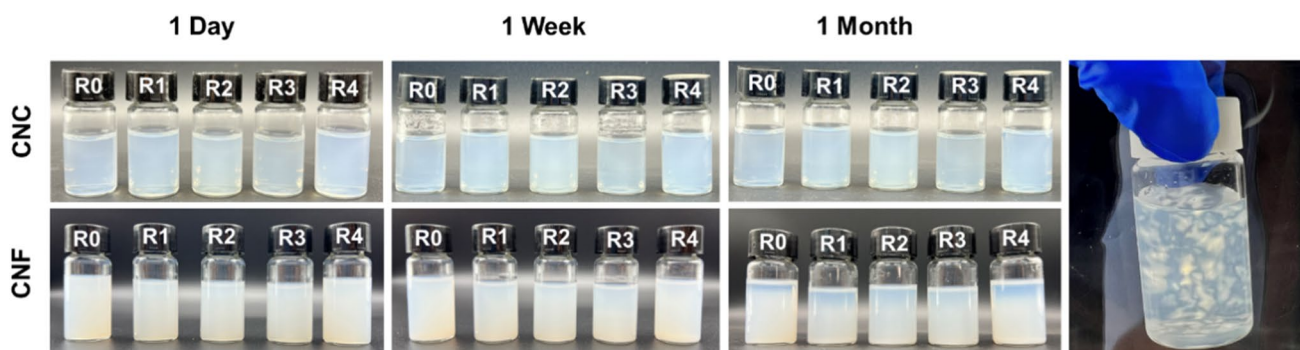


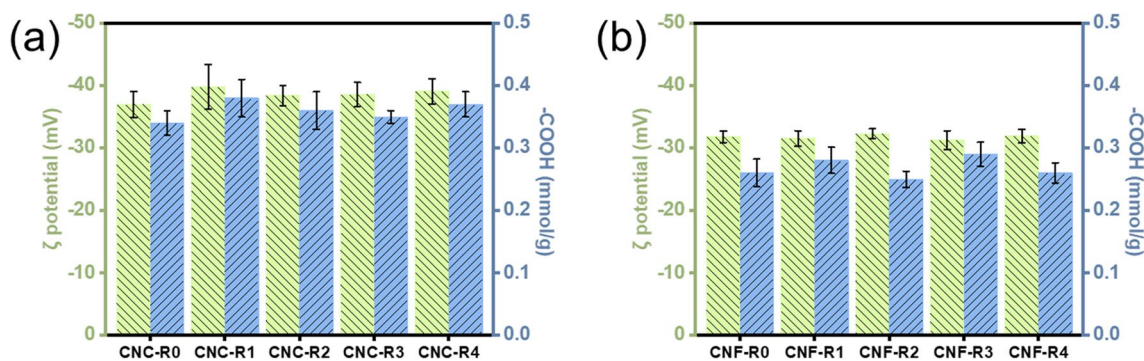
**Fig. 5** Photographs of CNC and CNF suspensions with different storage times. Flow birefringence phenomenon of CNC-R4 after 30-day storage (right)

even after standing for 1 month. In addition, it is clearly from left to right (increased cycles) at every stage that the dispersion stability of both CNC and CNF was not visible change, implying the excellent availability of OAD cyclic hydrolysis. Especially, typical flow birefringence phenomenon was still observed under cross-polarized light for CNC-R4 suspensions after 1 month of standing, as shown in Fig. 5 (right). However, CNF suspensions stratified to visible undergoing 30-day placement, which might be due to the larger size of CNF but the lower charge density. This would be proven by the results of zeta potential and carboxylic group contents of CNC and CNF.

From Fig. 6, all the CNC suspensions had a high charge density after OAD esterification with zeta potential values from  $-37$  to  $-40$  mV, proving a stable suspension [25]. CNF suspensions with the same concentration had a smaller absolute value of zeta potential ( $\sim 32$  mV) than that of CNC suspension, which was attributed to the lower carboxylic contents of CNF. TEM results in Fig. 4 had demonstrated that CNC had a smaller particle size, endowing CNC with larger contact surface area to sustain esterification reaction with OAD, acquiring higher carboxylic group contents. It is noteworthy that the recrystallization of OAD did not deteriorate its hydrolysis ability to WBP. Undergoing four recycles,

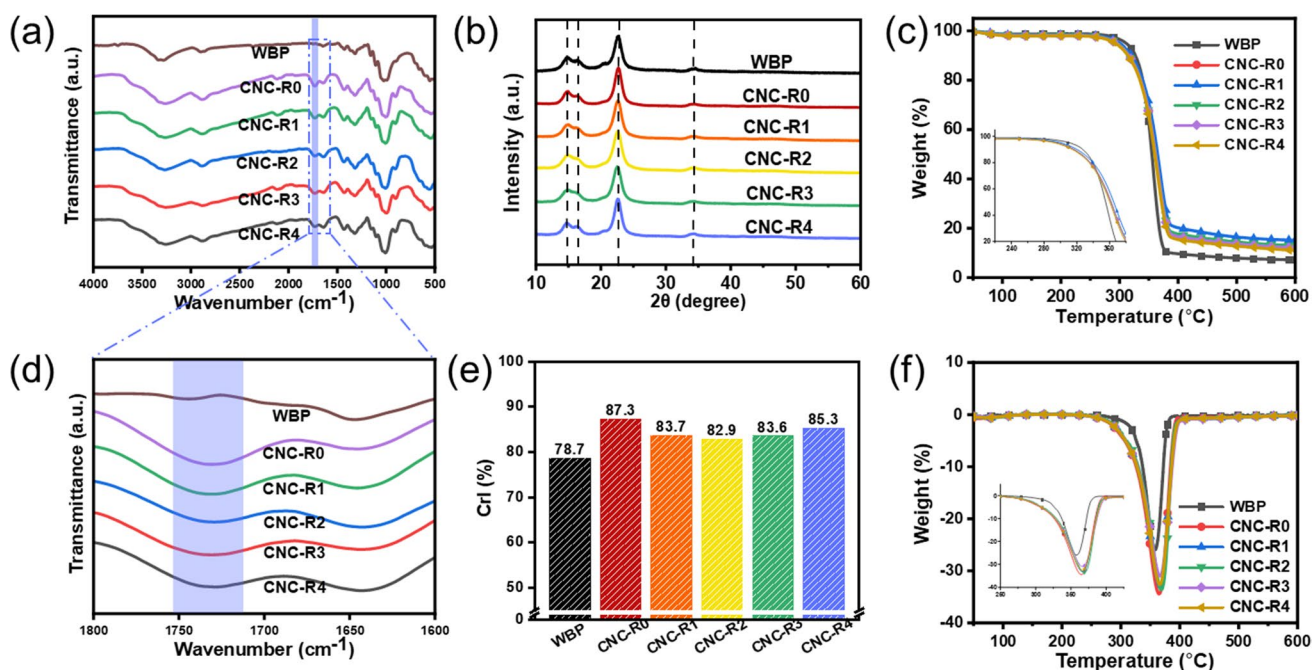
the carboxylic groups on CNC and CNF were around 0.37 and 0.26 mmol/g; there were no significant differences. All of the above results verified the validity of OAD recrystallization and recycle for WBP hydrolysis treatment, in which the obtained CNC and CNF not only had high yield but also had stable microstructure and surface characteristic. Therefore, in the following work, CNC as representative was selected to further evaluate the effect of OAD recycles on the chemical structure, crystal structure, and thermal stability.

Figure 7a, d shows the FTIR spectra of WBP and CNC-R<sub>x</sub> with different OAD recycles. Obviously, all samples had the characteristic absorption peaks of cellulose; the bands at 3300, 2880, 1425, 1049, and 895  $\text{cm}^{-1}$  were attributed to O–H stretching vibration, C–H stretching vibration, C–H bending vibration, C–O–C skeletal, and  $\beta$ -glycosidic linkage structure, respectively [10, 26]. This indicated that the basic structure of cellulose maintained unchanged during OAD hydrolysis. Differently, a new absorption peak at 1735  $\text{cm}^{-1}$  was detected on all CNC-R<sub>x</sub>, which could be ascribed to C=O stretching vibration involving in carboxylic group from cellulose esterification with OAD [27, 28]. Compared with original CNC-R0, no varied peaks appeared in other CNC-R<sub>x</sub>, demonstrating that multiple recycles of OAD did not create changes in the molecular structure of CNC.



**Fig. 6** Zeta potential and carboxyl group content of CNC-R<sub>x</sub> (a) and CNF-R<sub>x</sub> (b)





**Fig. 7** FTIR spectra (a, d), XRD patterns and CrI (b, e), and TG and DTG curves (c, f) of WBP and CNC-R<sub>x</sub>

The variation in crystal structure of WBP and CNC-R<sub>x</sub> with different OAD recycles was determined using XRD patterns, and shown in Fig. 7b, e. WBP and all CNC-R<sub>x</sub> possessed typical cellulose I crystalline phase with diffraction peaks at  $2\theta$  around  $14.8^\circ$ ,  $16.3^\circ$ ,  $22.7^\circ$ , and  $34.2^\circ$ , corresponding to  $(1\bar{1}0)$ ,  $(110)$ ,  $(200)$ , and  $(004)$  lattice plane, respectively [29]. Undergoing OAD hydrolysis, CrI of CNC-R<sub>0</sub> increased to 87.3% from 78.7% of WBP because of the successful removal of cellulose amorphous regions. OAD recycles had no effect on the peak position. Although a tiny declination, the crystalline fraction of cellulose was well retained, suggesting a good and stable processing ability of the proposed cyclic procedure.

The thermal stability of WBP and CNC-R<sub>x</sub> with different OAD recycles was also investigated by TGA, and shown in Fig. 7c, f. All CNC-R<sub>x</sub> had similar pyrolysis behaviors derived from their similar degree of crystallinity and functional group contents. The onset degradation temperature ( $T_{5\%}$ ) of CNC-R<sub>x</sub> was about  $295^\circ\text{C}$ , lower than that of WBP with  $310^\circ\text{C}$ , which was due to the priority degradation of ester carbonyl groups. In contrast, the maximum decomposition temperature ( $T_{\text{max}}$ ) and the residual mass at  $600^\circ\text{C}$  of CNC-R<sub>x</sub> were slightly increased owing to the relatively higher crystallinity than that of WBP. These results indicated the obtained CNC from OAD hydrolysis had excellent thermal stability. Although the onset degradation temperature is slightly lower than that of WBP, much higher than that of the CNC prepared by current sulfuric acid hydrolysis ( $221^\circ\text{C}$ ) [29] and TEMPO oxidation ( $227^\circ\text{C}$ ) [30] in Table S2.

In summary, CNC and CNF were efficiently extracted by the synergy strategy of OAD/ $\text{CrCl}_3$  hydrolysis and homogenization. It is well known that the recycle of OAD can significantly reduce the production costs. The combination of the above investigations demonstrated that the recrystallization and reuse of OAD had no significant influence on the yield, morphology, dispersion stability, surface functional groups, chemical and crystal structures, as well as thermal stability of CNC. Even undergoing four recycles, OAD still possessed admirably hydrolytic reactivity, could break intermolecular hydrogen bond interactions and cleave  $\beta$ -1-4-glycosidic bonds in cellulose chains, releasing nanocelluloses (Fig. S3) and retaining their morphology and chemical properties. Compared with most of previous reports in terms of preparation process, nanocellulose yield, and quality listed in Table S2, this work proved the applicability and the reliability of the proposed recyclable and stable strategy.

### 3.4 Scale production and economic evaluation

The high yield, recyclable, stable preparation process in this work provided a promising potential for large-scale production of nanocellulose including CNC and CNF. Therefore, pilot-scale production was enlarged to 30 L and conducted in a customized 50-L reactor under optimal conditions in Section 3.2 (Fig. S4). The total yield of CNC and CNF was about 90%, and displayed similar morphology and physicochemical properties with the above laboratory scale (Fig. S5). The produced CNC and CNF possessed high



crystallinity with CrI of 85.6 and 80.3%, and simultaneously have high surface carboxyl group content of 0.38 and 0.26 mmol/g, respectively. Further, the energy consumption and feedstock cost were counted, and the detailed statistics are shown in Table S3. Power consumption is 14.49 kWh/kg WBP in this strategy, much lower than that purely mechanical treatment (27–70 kWh/kg) [31, 32]. Moreover, the difference in costs was compared with or without the recycling process in terms of the cost of materials required to process each kilogram of WBP. It can be seen from Fig. S6 that the production cost is mainly concentrated on OAD cost, occupying 92.5% of the total cost without recycling process. The recrystallization and reuse of OAD significantly reduce the production costs to original 38.9%. In addition, ICP results showed no residue of Cr<sup>3+</sup> ions in CNC and CNF products (Table S4), verifying a green and safe method. Thus, the developed strategy in this work is a low cost, stable, and promising approach to manufacture nanocellulose materials. Currently, the natural cooling and recrystallization of OAD were carried out at room temperature; liquid wastes will be concentrated and reused in future work to further reduce the overall production cost.

## 4 Conclusions

In summary, carboxylic CNC and CNF were efficiently extracted from WBP via a recyclable and stable strategy of the combination of recyclable OAD hydrolysis with homogenization. RSM was conducted to optimize experimental variables to maximize CNC yield and achieved the optimum conditions with CNC yield of 58.6% when hydrolysis reaction was performed by 1.65 g/mL of OAD at 92 °C for 5.1 h. Importantly, manifold recrystallization-reuse cycles of OAD did not affect the yield, morphology, dispersion stability, surface functional groups, chemical and crystal structures, and thermal stability of CNC, demonstrating the applicability and the reliability of the proposed strategy. Further, the pilot-scale production of nanocellulose also verified the availability and high efficiency of the developed approach. The total yield of CNC and CNF was greater than 90%. The produced CNC and CNF had high crystallinity with CrI of 85.6 and 80.3%, and high carboxyl group content of 0.38 and 0.26 mmol/g, respectively. Moreover, the recycle of OAD significantly reduces the production costs of nanocellulose to original 38.9%. In addition, no residue of Cr<sup>3+</sup> ions were detected in CNC and CNF products. Therefore, this work not only provides a low cost and cyclically stable approach for manufacturing CNC and CNF but also provides high-performance nanocellulose, contributing to the high-value-added applications. Persistently, liquid wastes will be concentrated in our future work to explore the recycle of CrCl<sub>3</sub>,

hydrolyzed sugars, and water reuse for high value utilization of waste biomass.

**Supplementary Information** The online version contains supplementary material available at <https://doi.org/10.1007/s13399-024-05648-5>.

**Author contributions** Hanfei Zhao performed investigation, formal analysis, writing—original draft, and writing—review and editing. Longfei Sun, Jing Lu, and Xinxin Chen performed investigation and formal analysis. Yucong Yu performed structural characterization and analysis, and project support. Lin Liu performed conceptualization, writing—review, funding acquisition, and project administration.

**Funding** The work was financially supported by the National Natural Science Foundation of China (22375181) and Zhejiang Provincial Key Research and Development Program (2022C03093).

## Declarations

**Ethical approval** All authors are approving the final version of the manuscript to be published.

**Competing interests** The authors declare no competing interests.

## References

- Sun Y, Chu Y, Deng C, Xiao H, Wu W (2022) High-strength and superamphiphobic chitosan-based aerogels for thermal insulation and flame retardant applications. *Colloids Surf A Physicochem Eng Asp* 651. <https://doi.org/10.1016/j.colsurfa.2022.129663>
- Rivadeneira A, Marín-Sánchez A, Wicklein B, Salmerón JF, Castillo E, Bobinger M, Salinas-Castillo A (2021) Cellulose nanofibers as substrate for flexible and biodegradable moisture sensors. *Compos Sci Technol* 208. <https://doi.org/10.1016/j.compscitech.2021.108738>
- Yang S, Zhang Y, Zhang Y, Deng J, Chen N, Xie S, Ma Y, Wang Z (2023b) Designing Anti-swelling nanocellulose separators with stable and fast ion transport channels for efficient aqueous zinc-ion batteries. *Adv Funct Mater* 33(42). <https://doi.org/10.1002/adfm.202304280>
- Andrew LJ, Gillman ER, Walters CM, Lizundia E, MacLachlan MJ (2023) Multi-responsive supercapacitors from chiral nematic cellulose nanocrystal-based activated carbon aerogels. *Small* 19(34):e2301947. <https://doi.org/10.1002/sml.202301947>
- Pai AR, Lu Y, Joseph S, Santhosh NM, Degl'Innocenti R, Lin H, Letizia R, Paoloni C, Thomas S (2023) Ultra-broadband shielding of cellulose nanofiber commingled biocarbon functional constructs: a paradigm shift towards sustainable terahertz absorbers. *Chem Eng J* 467. <https://doi.org/10.1016/j.cej.2023.143213>
- Wagh RV, Khan A, Priyadarshi R, Ezati P, Rhim JW (2023) Cellulose nanofiber-based multifunctional films integrated with carbon dots and anthocyanins from Brassica oleracea for active and intelligent food packaging applications. *Int J Biol Macromol* 233:123567. <https://doi.org/10.1016/j.ijbiomac.2023.123567>
- Zhou M, Liao J, Li G, Yu Z, Xie D, Zhou H, Wang F, Ren Y, Xu R, Dai Y, Wang J, Huang J, Zhang R (2022) Expandable carboxymethyl chitosan/cellulose nanofiber composite sponge for traumatic hemostasis. *Carbohydr Polym* 294:119805. <https://doi.org/10.1016/j.carbpol.2022.119805>
- Liu Q, Li Q, Hatakeyama M, Kitaoka T (2023) Proliferation and differential regulation of osteoblasts cultured on surface-phosphorylated cellulose nanofiber scaffolds. *Int J Biol Macromol* 253(Pt 3):126842. <https://doi.org/10.1016/j.ijbiomac.2023.126842>

9. Mai T, Li DD, Chen L, Ma MG (2023) Collaboration of two-star nanomaterials: the applications of nanocellulose-based metal organic frameworks composites. *Carbohydr Polym* 302:120359. <https://doi.org/10.1016/j.carbpol.2022.120359>
10. Chen Z, Wan C (2018) Ultrafast fractionation of lignocellulosic biomass by microwave-assisted deep eutectic solvent pretreatment. *Bioresour Technol* 250:532–537. <https://doi.org/10.1016/j.biortech.2017.11.066>
11. Jiang J, Zhu Y, Jiang F (2021a) Sustainable isolation of nanocellulose from cellulose and lignocellulosic feedstocks: recent progress and perspectives. *Carbohydr Polym* 267:118188. <https://doi.org/10.1016/j.carbpol.2021.118188>
12. Qi Y, Guo Y, Liza AA, Yang G, Sipponen MH, Guo J, Li H (2023) Nanocellulose: a review on preparation routes and applications in functional materials. *Cellulose* 30(7):4115–4147. <https://doi.org/10.1007/s10570-023-05169-w>
13. Yang C, Zhu Y, Tian Z, Zhang C, Han X, Jiang S, Liu K, Duan G (2023a) Preparation of nanocellulose and its applications in wound dressing: a review. *Int J Biol Macromol* 254(Pt 3):127997. <https://doi.org/10.1016/j.ijbiomac.2023.127997>
14. Jia W, Liu Y (2019) Two characteristic cellulose nanocrystals (CNCs) obtained from oxalic acid and sulfuric acid processing. *Cellulose* 26(15):8351–8365. <https://doi.org/10.1007/s10570-019-02690-9>
15. Chen L, Zhu JY, Baez C, Kitin P, Elder T (2016) Highly thermal-stable and functional cellulose nanocrystals and nanofibrils produced using fully recyclable organic acids. *Green Chem* 18(13):3835–3843. <https://doi.org/10.1039/c6gc00687f>
16. Ji H, Xiang Z, Qi H, Han T, Pranovich A, Song T (2019) Strategy towards one-step preparation of carboxylic cellulose nanocrystals and nanofibrils with high yield, carboxylation and highly stable dispersibility using innocuous citric acid. *Green Chem* 21(8):1956–1964. <https://doi.org/10.1039/c8gc03493a>
17. Jiang J, Zhu Y, Zargar S, Wu J, Oguzlu H, Baldelli A, Yu Z, Sadtler J, Sun R, Tu Q, Jiang F (2021b) Rapid, high-yield production of lignin-containing cellulose nanocrystals using recyclable oxalic acid dihydrate. *Ind Crop Prod* 173. <https://doi.org/10.1016/j.indcrop.2021.114148>
18. Henschen J, Li D, Ek M (2019) Preparation of cellulose nanomaterials via cellulose oxalates. *Carbohydr Polym* 213:208–216. <https://doi.org/10.1016/j.carbpol.2019.02.056>
19. Liu W, Du H, Liu H, Xie H, Xu T, Zhao X, Liu Y, Zhang X, Si C (2020) Highly efficient and sustainable preparation of carboxylic and thermostable cellulose nanocrystals via FeCl<sub>3</sub>-Catalyzed innocuous citric acid hydrolysis. *ACS Sustain Chem Eng* 8(44):16691–16700. <https://doi.org/10.1021/acssuschemeng.0c06561>
20. Tang F, Li Y, Huang J, Tang J, Chen X, Yu H-Y, Zhou Y, Tang D (2021) An environmentally friendly and economical strategy to cyclically produce cellulose nanocrystals with high thermal stability and high yield. *Green Chem* 23(13):4866–4872. <https://doi.org/10.1039/d1gc01392k>
21. Shang Z, An X, Seta FT, Ma M, Shen M, Dai L, Liu H, Ni Y (2019) Improving dispersion stability of hydrochloric acid hydrolyzed cellulose nano-crystals. *Carbohydr Polym* 222:115037. <https://doi.org/10.1016/j.carbpol.2019.115037>
22. Peng H, Yuan L, Zhang J, Wu X, Liu Y, Liu Y, Ruan R (2018) Adsorption of AgNO<sub>3</sub> onto bamboo hemicelluloses in aqueous medium. *Carbohydr Polym* 188:8–16. <https://doi.org/10.1016/j.carbpol.2018.01.051>
23. Chen YW, Lee HV, Abd Hamid SB (2017) Investigation of optimal conditions for production of highly crystalline nanocellulose with increased yield via novel Cr(III)-catalyzed hydrolysis: response surface methodology. *Carbohydr Polym* 178:57–68. <https://doi.org/10.1016/j.carbpol.2017.09.029>
24. Wang L, Zhu X, Chen X, Zhang Y, Yang H, Li Q, Jiang J (2022) Isolation and characteristics of nanocellulose from hardwood pulp via phytic acid pretreatment. *Ind Crop Prod* 182. <https://doi.org/10.1016/j.indcrop.2022.114921>
25. Yang X, Xie H, Du H, Zhang X, Zou Z, Zou Y, Liu W, Lan H, Zhang X, Si C (2019) Facile extraction of thermally stable and dispersible cellulose nanocrystals with high yield via a green and recyclable FeCl<sub>3</sub>-Catalyzed deep eutectic solvent system. *ACS Sustain Chem Eng* 7(7):7200–7208. <https://doi.org/10.1021/acsschemeng.9b00209>
26. Zhao J, Deng M, Li S, Guan Z, Xia Y, Yang J, Lin X (2022) Room temperature preparation of cellulose nanocrystals with high yield via a new ZnCl<sub>2</sub> solvent system. *Carbohydr Polym* 278:118946. <https://doi.org/10.1016/j.carbpol.2021.118946>
27. Robles E, Izaguirre N, Dogaru B-I, Popescu C-M, Barandiaran I, Labidi J (2020) Sonochemical production of nanoscaled crystalline cellulose using organic acids. *Green Chem* 22(14):4627–4639. <https://doi.org/10.1039/d0gc01283a>
28. Liu Y, Zhang S, Lin R, Li L, Li M, Du M, Tang R (2021) Potassium permanganate oxidation as a carboxylation and defibrillation method for extracting cellulose nanofibrils to fabricate films with high transmittance and haze. *Green Chem* 23(20):8069–8078. <https://doi.org/10.1039/d1gc02657g>
29. Kassab Z, Syafri E, Tamraoui Y, Hannache H, Qaiss AEK, El Achaby M (2020) Characteristics of sulfated and carboxylated cellulose nanocrystals extracted from *Juncus* plant stems. *Int J Biol Macromol* 154:1419–1425. <https://doi.org/10.1016/j.ijbiomac.2019.11.023>
30. Zhang K, Sun P, Liu H, Shang S, Song J, Wang D (2016) Extraction and comparison of carboxylated cellulose nanocrystals from bleached sugarcane bagasse pulp using two different oxidation methods. *Carbohydr Polym* 138:237–243. <https://doi.org/10.1016/j.carbpol.2015.11.038>
31. Osong SH, Norgren S, Engstrand P (2015) Processing of wood-based microfibrillated cellulose and nanofibrillated cellulose, and applications relating to papermaking: a review. *Cellulose* 23(1):93–123. <https://doi.org/10.1007/s10570-015-0798-5>
32. Ang S, Haritos V, Batchelor W (2019) Effect of refining and homogenization on nanocellulose fiber development, sheet strength and energy consumption. *Cellulose* 26(8):4767–4786. <https://doi.org/10.1007/s10570-019-02400-5>

**Publisher's Note** Springer Nature remains neutral with regard to jurisdictional claims in published maps and institutional affiliations.

Springer Nature or its licensor (e.g. a society or other partner) holds exclusive rights to this article under a publishing agreement with the author(s) or other rightsholder(s); author self-archiving of the accepted manuscript version of this article is solely governed by the terms of such publishing agreement and applicable law.